Multialkali phosphate glasses: A new window to understand the mechanism of ion transport*

K. J. Rao† and Sundeep Kumar

Solid State and Structural Chemistry Unit, Indian Institute of Science, Bangalore 560 012, India

Alkali metaphosphate glasses containing two and three alkalis have been prepared by melt-quenching method over a wide range of compositions. Several properties of these glasses such as density, molar volume, glass transition temperature, heat capacity jump and NMR chemical shift of ^{31}P, ^{23}Na and ^{7}Li nuclei have been measured. Transport properties have been studied over a wide range of frequency and temperature. Mixed alkali effect (MAE), which manifests in three alkali-containing glasses is found to be complex. Arrhenius plots of d.c. conductivities are characterized by two slopes and a.c. conductivities display two power-law regimes with two characteristic *s* values. The imaginary part of the electric modulus exhibits a unique two-peak relaxation behaviour and the peaks merge at higher temperatures. This is first time such a behaviour has been observed in a.c. conductivity and dielectric relaxation of glasses. A new mechanism has been proposed to understand ion transport in oxide glasses, which rationalizes all the observations made in the trialkali phosphate system examined here.

A widely investigated phenomenon in glasses is the so-called mixed alkali effect (MAE)[1–3]. Glasses containing two alkalis exhibit highly nonlinear variations of properties when one alkali is systematically substituted by the other. The effect is most clearly manifest in the measured ionic conductivity and diffusion coefficient of glasses. Conductivity generally exhibits a minimum in mixed-alkali glasses. The same behaviour is often exhibited when the alkali ion is substituted by an isovalent non-alkali ion also, and is referred to as mixed-ion effect. The nonlinear behaviour is also observed in several properties such as molar volume (logarithmic) viscosity (ln h) isokom, viscosity activation barrier (E_h), kinetic fragility ($F_{1/2}$, estimated using viscosity data), dielectric constant (e'), dielectric loss (tan d), etc. The origin of MAE has been attributed to structural[4], electrodynamic[5] and other[3,6–8] factors. More recently, MAE has been investigated using computer simulation. Monte Carlo[9], molecular dynamics[10] and reverse Monte Carlo[11] techniques have all been used in such studies. It appears that alkali-ion migration occurs through preferred pathways[9,10] in the glass structure, and these pathways are the loci of like-ion sites. One alkali does not utilize the pathway of the other due to unfavourable energetics[9,10,12]. When two alkalis are present, blocking of each other's path or formation of discontinuities in the pathways are found to be responsible for diminished conductivity[10].

None of the experiments seems to directly reveal this blocking effect. DC conductivity measurement indicates the presence of single activation barrier in spite of the presence of two alkalis which follow independent paths. AC conductivity reveals that the values vary simply $\sim A + Bw^s$ and with a single characteristic s (A and B are constants). Dielectric studies also reveal that there is only one relaxation peak, which can be fitted with a stretched exponential function with a characteristic b. We have recently[13] analysed MAE in a complex borotellurate glass and traced this behaviour to the nature of the conduction mechanism itself, and have argued that the conduction involves two steps. The first one is non-bridging oxygen (NBO) migration through a BO–NBO switching (BO stands for bridging oxygen) followed by the second step which is the alkali-ion migration. The measured barriers refer to BO–NBO activation. The observed maxima in activation barriers is due to additional hindrance to BO–NBO switching offered by the presence of dissimilar alkalis in the environment of the BO–NBO pairs.

In this article we analyse this approach further by investigating a system of glasses containing single network former but with two and three alkalis. Addition of a third alkali to a system containing two alkalis immediately leads to the presence of three pairs of alkalis. Correspondingly, compositions that could be prepared and studied also increase in number. We have presented in this investigation, two series of glasses in Li_2O-Na_2O-K_2O containing metaphosphate glass system; one containing no Li_2O (two alkalis) and the other containing constant – 10 mol% – Li_2O (three alkalis). We have examined a number of properties, including density and molar volume, glass transition temperature, heat capacity, HR MAS–NMR of ^{7}Li, ^{23}Na and ^{31}P nuclei, d.c. conductivity and dielectric relaxation. The results have been discussed with a focus on the insights that they provide regarding ion transport in glasses.

Experimental

Glasses were prepared by the conventional melt-quenching method. Ten gram batches of the starting materials, Li_2CO_3 (Qualigens), Na_2CO_3 (Qualigens), K_2CO_3 (Quali-

*Dedicated to Prof. S. Ramaseshan on his 80th birthday.

†For correspondence. (e-mail: kjrao@sscu.iisc.ernet.in)

gens) and $(NH_4)_2HPO_4$ (Aldrich) (all of Analar grade) were mixed thoroughly by repeated grinding. The ground mixtures were heated in platinum crucibles at 673 K for about 5 h in a muffle furnace to decompose Li_2CO_3, Na_2CO_3, K_2CO_3 and $(NH_4)_2HPO_4$. The batches were then melted at 1173 K for about 10 min, stirred to ensure homogeneity and quenched between stainless-steel plates kept at room temperature.

The amorphous nature of the glass samples was confirmed using X-ray diffraction (CuK_a Siemens D-5005, Germany). That the products were truly glasses was ascertained by the observation of glass transition in them using Differential Scanning Calorimetry (DSC; Perkin-Elmer DSC-2). Thermal properties like glass transition temperature T_g and heat capacity C_p of the samples were also determined. Dry nitrogen was used as purge gas during DSC experiments. The C_p of the glasses was determined from room temperature up to temperatures well above T_g (limited only by the incidence of crystallization) using corresponding DSC data on a piece of single-crystal sapphire (Al_2O_3; standard). The density was determined using glass bits free of air bubbles and cracks (in 10 × magnification) through apparent weight loss method. Xylene was used as the immersion fluid. Measured density of well-annealed glasses was found to be accurate and reproducible to ± 0.001 g/cc. The molar volume $V_m = (W_m/\text{density})$, was calculated from density data, W_m being the corresponding formula weights.

^{7}Li, ^{23}Na and ^{31}P HR MAS–NMR spectra were recorded on a Bruker MSL-300 (magnetic field 7.05 T) solid-state high-resolution spectrometer operating at 116.64 MHz (for ^{7}Li), 79.34 MHz (for ^{23}Na) and 121.50 MHz (for ^{31}P). In all the experiments 90° pulses of 5 μs were employed with a delay time of 10 s between pulses. A spinning speed of 7–10 kHz was employed. All the spectra were recorded at room temperature using freshly-powdered samples. The standards used for the evaluation of chemical shifts of ^{7}Li, ^{23}Na and ^{31}P in glasses have been standard aqueous solutions of LiCl, NaCl and H_3PO_3, respectively.

Electrical-conductivity measurements were carried out on a Hewlett–Packard HP 4192A LF impedance-gain phase analyser (Hewlett–Packard, USA) from 10 Hz to 13 MHz in the temperature range of 298 to 600 K. A home-built cell assembly (having a 2-terminal capacitor configuration and silver electrodes) was used for the measurements. The sample temperature was measured using a Pt–Rh thermocouple positioned close to the sample. The temperature was controlled using a Heatcon (Bangalore, India) temperature controller and temperature constancy of ± 1 K was achieved in the entire range of measurements. Annealed circular glass bits coated with silver paint on both sides and having thickness of about 0.1 cm and 1 cm diameter, were used for measurements.

The real (Z') and imaginary (Z'') parts of the complex impedance (Z^*) were obtained from the measured conductance and capacitance using the relations

$$Z' = \left(\frac{G}{G^2 + w^2 C^2} \right),$$

$$Z'' = \left(\frac{wC}{G^2 + w^2 C^2} \right),$$

where G is the conductance, C the parallel capacitance, and w (= $2pf$) is the angular frequency, where f is the frequency of the a.c. field. The real (e') and imaginary (e'') parts of the complex dielectric constant were calculated from the relations

$$e' = \frac{Cd}{e_0 A},$$

$$e'' = \frac{s}{we_0},$$

where d is the sample thickness, A the cross-sectional area, s the conductivity, and e_0 the permittivity of free space.

The data were also analysed using the electrical modulus formalism. The real (M') and imaginary (M'') parts of the complex electrical modulus ($M^* = 1/e^*$) were obtained from e' and e'' values using the relation

$$M' = \frac{e'}{(e')^2 + (e'')^2},$$

$$M'' = \frac{e''}{(e')^2 + (e'')^2},$$

Results

Glasses investigated here correspond to the general formula $(M_1, M_2, M_3)_2O \cdot P_2O_5$. The actual compositions of the two series of glasses are given in Table 1. The first series (series A) is simple mixed (two) alkali glasses containing Na_2O and K_2O, while the second series (series B) is multi-alkali glasses albeit with a fixed Li_2O concentration of 10 mol% (20 mol% of total alkali). In both the series, the glass-forming network is that of metaphosphate which ideally corresponds to a structure of infinite self-entangled chains. (Metaphosphates can often be disproportionate, but this possibility is ignored in this article.) In the following discussion, glasses are referred as $(x_1 : x_2 : x_3)$, where x_1, x_2 and x_3 refer to the mole percentages of Li_2O, Na_2O and K_2O, respectively in the glass composition. Density and molar volume for all the glasses have been listed in Table 1. The measured density and molar volume are shown in Figure 1 *a* and *b* for series A. The *x*-axis is represented by the mixed-alkali parameter, which is the mole fraction of one of the alkalis divided by the sum of the mole fractions of both the alkalis. Thus the mixed-alkali parameter varies from 0 to 1. In Figure 1 *c* and *d*, variations of density

and molar volume are shown for series B as a function of the same mixed-alkali parameter used in Figure 1 *a* and *b*. This enables evaluation of the influence of introducing a constant concentration of a third alkali, namely Li_2O. Variations of T_g and ΔC_P – the magnitude of heat capacity jump at T_g – are shown in Figure 2 *a* and *b* for series A and in Figure 2 *c* and *d* for series B, respectively T_g and ΔC_P are defined in Figure 2 *c* (inset) using a typical heat capacity plot. The values of T_g and ΔC_P have also been listed in Table 1. The NMR chemical shifts of ^{23}Na and ^{31}P are similarly shown for series A in Figure 3 *a* and *b* and for series B in Figure 3 *c* and *d*, respectively. The behaviour of ^{7}Li chemical shift in series B is shown in Figure 3 *e*. Variations of logarithmic d.c. conductivity at 423 K and the conductivity activation barriers (E_{dc}) are shown as functions of mixed-alkali parameter in Figures 4 *a* and *b* for series A, and in Figure 4 *c* and *d* for series B, respectively. Values of s_{dc} at 423 K and E_{dc} for all the glasses have been listed in Table 1. For a majority of glasses investigated, the d.c. conductivity could be determined using Nyquist plots (Z'' vs Z'); a typical example is shown in Figure 4 *a* (inset). In those cases where the semicircles in the complex impedance plots were not satisfactory, s_{dc} values were determined from an extrapolation towards $w = 0$ of the a.c. conductivity in log $s(w)$ vs log w plots (based on the assumption, $s_{dc} = s(0)$). A typical log $s(w)$ vs log w plot is shown in Figure 4 *c* (inset). The temperature behaviour of the d.c. conductivity in series A and series B was found to exhibit significant differences. While the Arrhenius plots were quite linear in series A, in series B these plots indicated the presence of at least two slopes, and high temperature slopes (activation energies) exhibited significantly low values. In Figure 5 *a* and *b*, Arrhenius plots are shown for two typical compositions. The trialkali glasses, therefore, do not exhibit simple Arrhenius behaviour.

The a.c. conductivities of all the glasses were analysed using Almond–West-type[14–16] single-exponent power law. Typical plots are shown in Figure 6 *a* for a few of the series-A glasses measured at various temperatures. The a.c. conductivity of the end members of series B gave good Almond–West plots. The trialkali compositions indicated the presence of two distinct slopes in the frequency-dependent region. Typical behaviour is shown in Figure 6 *b*, where this behaviour is quite well-displayed and has the trialkali composition (10 : 20 : 20) from series B. The relaxation behaviour has been examined using plots of dielectric modulii vs logarithmic frequency. Typical plots for series-A glasses which exhibit classical M' dispersion and M'' peaks are shown in Figure 7 *a* and *b*, respectively at various temperatures. The behaviour of the trialkali glasses of series B was again different (Figure 7 *c* and *d*). They exhibit step-like dispersion of M' and either a broad peak or twinned peaks in M'' plots. These are shown for the case of (10 : 20 : 20) glass from series B for various temperatures, where such a behaviour is pronounced. As the temperature is increased, the two relaxation peaks get merged into a single M'' peak typical of bialkali glasses and step-like behaviour in M' dispersion also disappears. The behaviour exhibited in Figures 6 and 7 has implications for the transport mechanism, which is discussed in the next section.

Discussion

Density and molar volume

Figure 1 *a* indicates that in bialkali glasses of series A, density is insensitive to the substitution of Na_2O by K_2O. However, the presence of 10 mol% Li_2O removes this density insensitivity to the substitution of Na_2O by K_2O. Molar volume behaviour is nonlinear in both series of glasses. In series B, the presence of 20 mol% (of the total alkali) Li_2O appears to affect the molar volume significantly. At the potassium end, comparison of Figure 1 *b* and *d* suggests that the molar volume decrease can be as high as 2.14 cc. The implication of this for the structure

Table 1. Composition of glasses (P_2O_5 content is constant (50 mol%) in all the glasses), densities, molar volume, T_g, ΔC_P, $F_{1/2}$, d.c. conductivity at 423 K, activation barrier (E_{dc}), and diffusionless activation barrier (W)

Series	Li_2O	Na_2O	K_2O	Density (g/cc)	Molar volume (cc)	T_g (K)	ΔC_P (J mol^{-1} K^{-1})	$F_{1/2}$	s_{dc} (S cm^{-1})	E_{dc} (eV)	W(eV)
A	00	50	00	2.49	40.95	546	51.60	0.53	6.98×10^{-7}	0.84	0.84
	00	40	10	2.49	42.31	501	52.00	0.52	1.00×10^{-8}	1.10	1.39
	00	30	20	2.49	43.68	489	51.00	0.56	5.23×10^{-8}	0.91	0.97
	00	20	30	2.46	45.59	472	48.46	0.51	8.77×10^{-8}	0.88	0.95
	00	10	40	2.44	47.36	477	41.05	0.51	4.55×10^{-9}	1.25	1.29
	00	00	50	2.43	48.95	491	60.65	0.37	2.59×10^{-8}	1.06	1.1
B	10	00	40	2.40	46.81	487	47.55	0.51	3.25×10^{-6}	1.10	1.06
	10	10	30	2.44	44.65	473	48.00	0.53	1.07×10^{-7}	0.55	0.48
	10	20	20	2.46	42.90	480	50.83	0.48	2.00×10^{-8}	1.02	1.20
	10	30	10	2.47	41.36	479	56.40	0.39	6.02×10^{-9}	1.50	1.53
	10	40	00	2.48	39.82	520	41.85	0.60	1.49×10^{-8}	1.20	1.25

of the glass is that the metaphosphate chains surround the alkali ions as effectively as possible and lead to efficient packing in the glassy state. This can be contrasted with the interalkali substitution in crystalline NASICONs of fairly rigid structure of the phosphate matrix, where interalkali substitution has hardly any effect on molar volumes[17]. More important for the subject of this article is the observation of effective packing around the alkali ions, which can affect alkali-ion transport.

Thermal and NMR studies and glass structures

Variation of glass transition temperatures as a function of mixed-alkali parameter is also unusual for glasses of series B. By comparing Figure 2 *a* and *c*, it is seen that at the sodium end T_g decreases significantly, while at the K_2O end it is not much affected. This is caused by the substitution of 20% Na_2O or K_2O by Li_2O. The ^7Li NMR chemical shifts (see Figure 3 *e*) reveal that lithium is far less shielded in the sodium glass than in the potassium glass. The greater shielding is suggestive of significant degree of covalent bonding of Li with the cage oxygen ions. Therefore, Li^+ ions at the potassium end of composition in series B are relatively immobilized, while at the sodium end Li^+ ions are relatively free. Thus in the sodium end compositions, the presence of two alkalis suppresses liquidus temperature and hence the T_g (assuming the general validity of $T_g/T_m = 2/3$)[3] by virtue of increasing the configurational entropy. At the potassium end, the relatively immobilized Li^+ ions may not contribute to the configurational entropy, as a result of which T_g is not

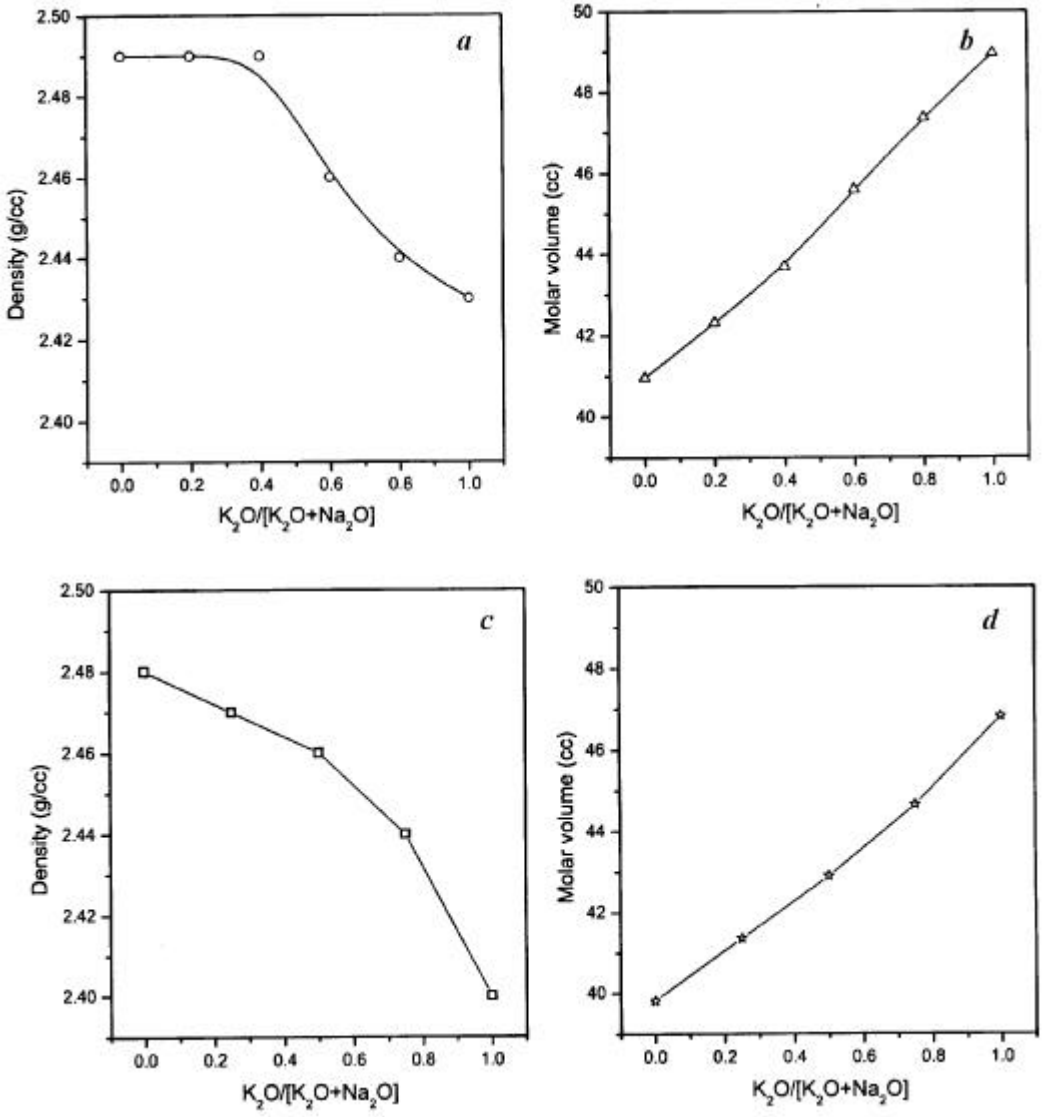

Figure 1. Variation of density (***a***) and molar volume (***b***) of glasses in series A as a function of mixed-alkali parameter. Variation of density (***c***) and molar volume (***d***) of glasses in series B as a function of the same mixed-alkali parameter.

much affected at the potassium end. The variation of T_g however, exhibits inflections in the intermediate compositions in series A and series B (Figure 2). This is indicative of the formation of some preferred structural groupings as the melt is cooled towards T_g. In the absence of any clear collateral evidence of phase separation, we wish to consider this as a consequence of cluster formation due to compositional fluctuations, which can readily occur in these multi-alkali glasses. Formation of clusters or such preferred structural groupings is supported by the behaviour of ^{23}Na chemical shifts (Figure 3 *a* and *c*). The chemical-shift variation in series A shows that the addition of Li_2O leads to a deshielding of ^{23}Na. Since Li^+ is a smaller ion, it may polarize electron clouds of the shared NBOs (alkali ions are generally known to be located close to NBOs in glass structures; see later) and therefore deshield Na^+ ions. The ^{23}Na deshielding continues to increase, although to a small extent towards the potassium end. This is understandable since molar volumes increase towards the potassium end (Figure 1 *d*) and the Na^+ ions therefore occupy slightly expanded voids, where they are even less shielded. The effect of Li^+ should be expected to be similar on the ^{31}P chemical shifts at sodium and potassium-end compositions. Indeed, they are affected significantly in the end compositions, as seen from Figure 3 *b* and *d*. In the trialkali compositions, it appears that the formation of structural groupings as indicated earlier, affects the behaviour of chemical shifts profoundly. First of all, the formation of structural groupings is generally dictated by local stoichiometries which tend to be close to those of stable crystalline phases.

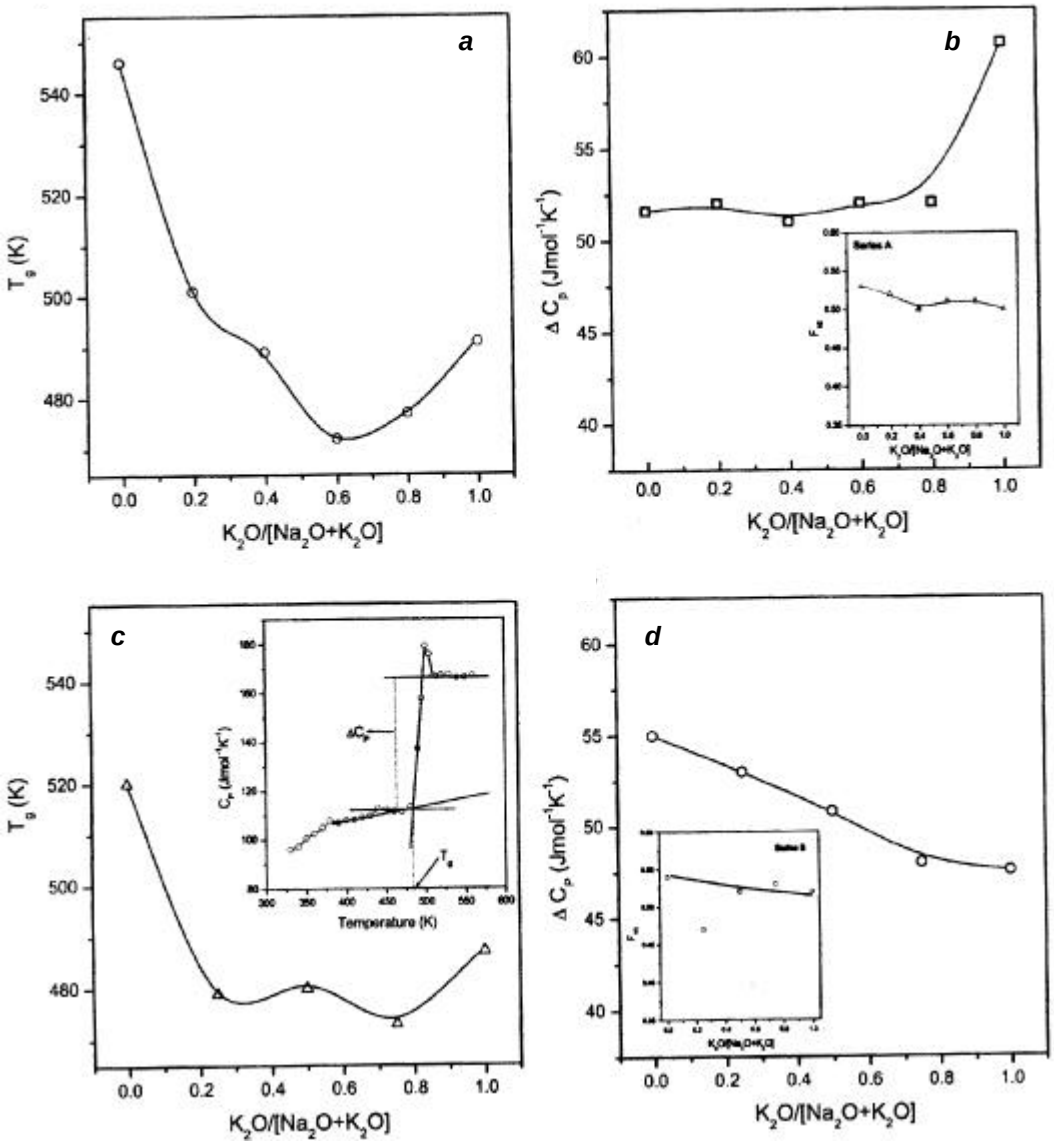

Figure 2. Variation of T_g (***a***) and ΔC_P (***b***) as a function of mixed-alkali parameter for glasses in series A, and variation of T_g (***c***) and ΔC_P (***d***) as a function of mixed-alkali parameter for glasses in series B. (Inset; ***c***) Typical heat capacity plot used in determining various thermal parameters. Thermodynamic fragilities have been shown as a function of mixed-alkali parameter in insets to ***b*** and ***d***.

In such structural groupings, ordering energy values are more likely to be higher than the entropy terms and the result is that the alkali ions – and in particular, Li^+ ions – are forced to occupy voids of rigid configurations in which their ability to polarize electron clouds and hence affect the chemical shifts are suppressed. Therefore, the chemical shifts are restored to the levels observed when Li^+ is absent (Figure 3 *b*).

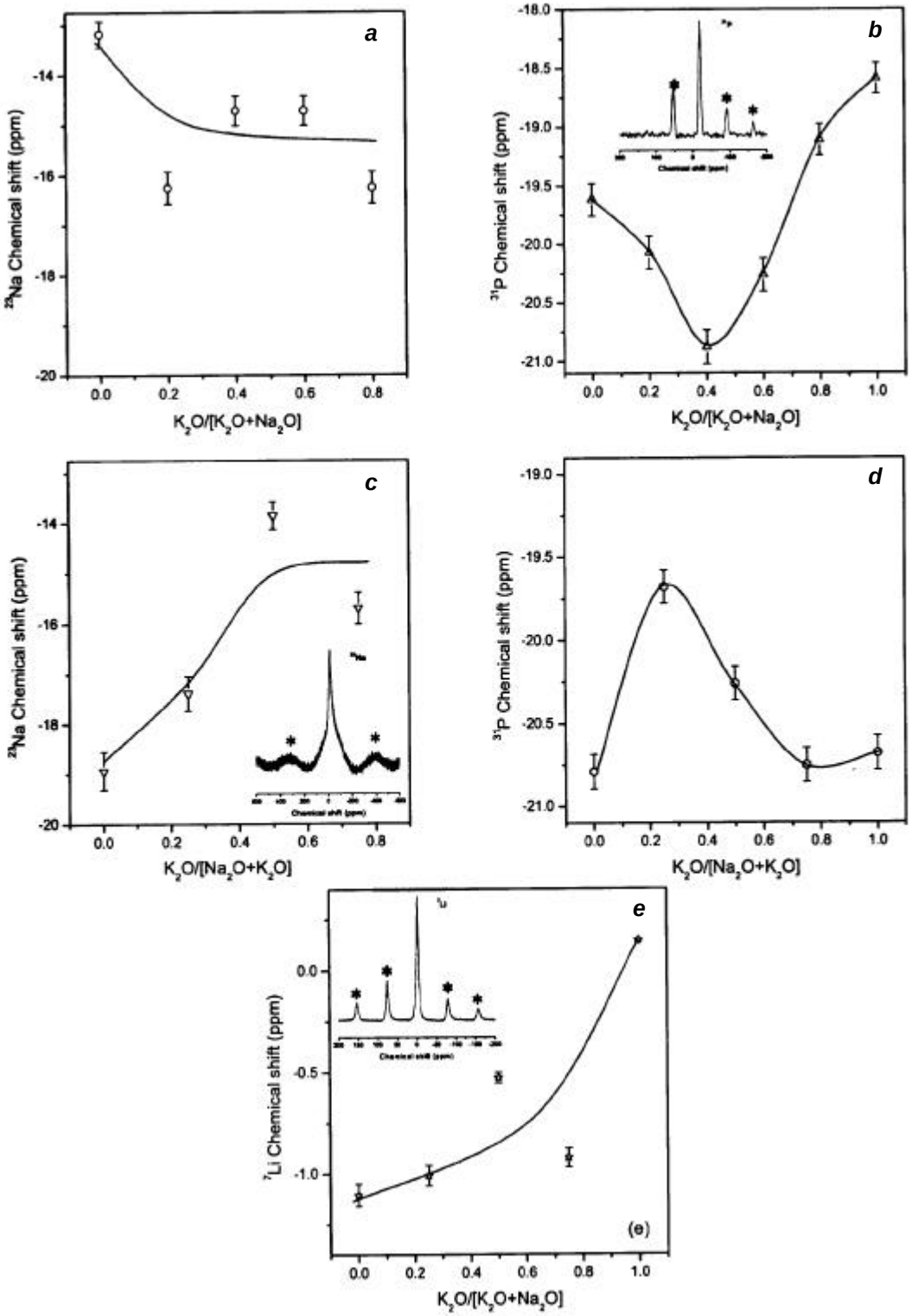

Figure 3. Variation of chemical shifts in series A: (***a***) for ^{23}Na; (***b***) for ^{31}P; in series B: (***c***) for ^{23}Na, (***d***) for ^{31}P and (***e***) for ^{7}Li. The *x*-axis is mixed-alkali parameter. (Inset) ***b***, ***c*** and ***e***, Typical HR MAS–NMR spectra for ^{23}Na, ^{31}P and ^{7}Li, respectively. The starred peaks indicate side bands.

The magnitudes of heat capacity jumps at T_g are generally indicative of the nature of bonding in the glasses[3]. Higher degree of covalency of bonding in glasses is associated with lower values of ΔC_P; higher values of ΔC_P are generally suggestive of higher degree of ionic bonding. Variations of ΔC_P observed in both the series of glasses are interesting. In Li_2O-free glasses (series A), ΔC_P values are generally high and rise to higher values towards the potassium end. Therefore, in potassium metaphosphate glass, bonding appears to be distinctly more ionic than in sodium metaphosphate glass. In series B, presence of Li_2O generally suppresses the value of ΔC_P towards the potassium end, indicating increased average covalency of bonding. However, in Na_2O-rich glasses, the actual ΔC_P values are somewhat higher. Increased covalency in K_2O-rich glasses is also reflected in the calculated values of thermodynamic $F_{1/2}$ fragilities, which were determined using the formula[18],

$$F_{1/2} = \frac{0.151 - x}{0.151 + x},$$

where $x = \Delta T_g/T_g$ and ΔT_g is the width of the glass transition. $F_{1/2}$ values for all the glasses have been listed in Table 1. Fragilities are generally high for Li_2O-free glasses of series A compared to Li_2O-containing glasses. This behaviour of fragility is shown in Figure 2 *b* and *d* (inset).

Transport studies

As noted earlier, d.c. conductivity was determined by analysing a.c. conductivity measured over a frequency range of 10 Hz to 12 MHz, both using Nyquist and Almond–West plots[14–16]. DC conductivity behaviour shown in Figure 4 *a* for series A indicates that the conductivity at the sodium

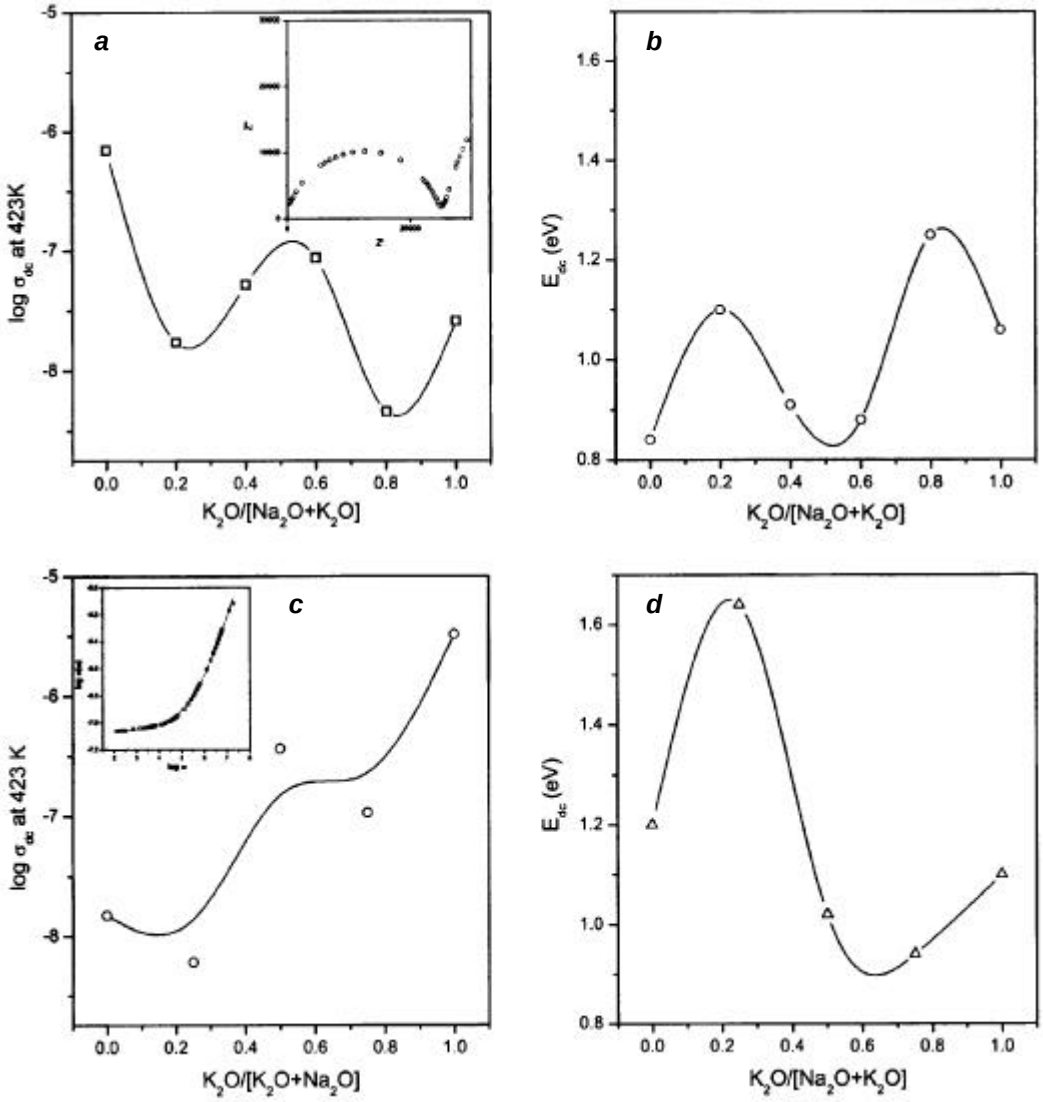

Figure 4. Behaviour of d.c. conductivity for glasses in series A; (***a***) and series B (***c***). Variation of activation barriers for glasses in series A (***b***) and series B (***d***). (Inset) ***a***, ***c***, Typical Nyquist plot and Almond–West plot, respectively.

end is higher than that at the potassium end, and conductivity *does not exhibit a single minima* in these glasses. The corresponding activation barrier values are shown in Figure 4 *b*. A cursory analysis reveals that the activation barriers are the determining factors for conductivity and therefore the influence of the preexponential factor is less important for our purpose. It would also appear that the end points correspond to transport of Na^+ and K^+ ions, and that s_{dc} of K^+ ion is understandably lower than that of the Na^+ ion because of its larger size and higher mass. The presence of a maximum in between would also be consistent, if the glass structure is constituted of ordered clusters of some – as yet unclear – description and with compositions nearly that of $(Na\text{-}K)(PO_3)_2$. Such clusters are likely to possess higher intrinsic alkali-ion conductivities. On the whole, it would appear that the system (see Figure 4 *a*

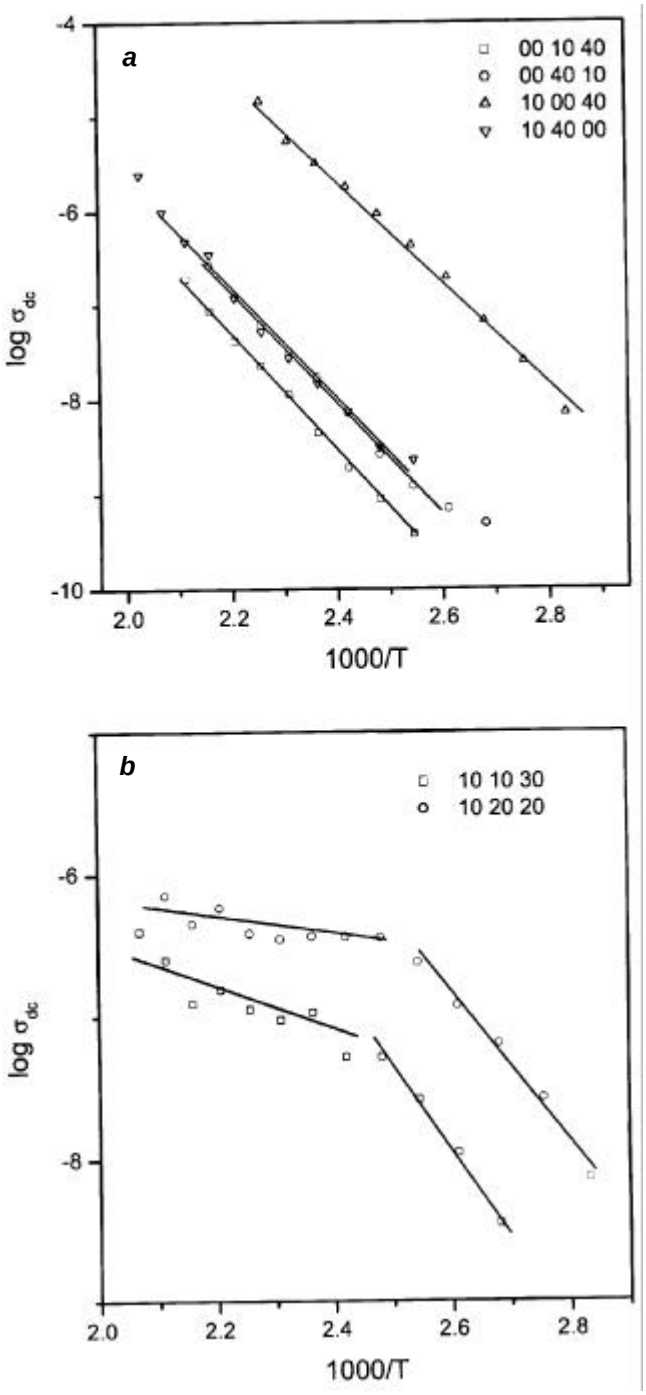

Figure 5. ***a***, Arrhenius plot for typical bialkali glasses from series A and series B. ***b***, Arrhenius behaviour of two trialkali-containing glasses from series B.

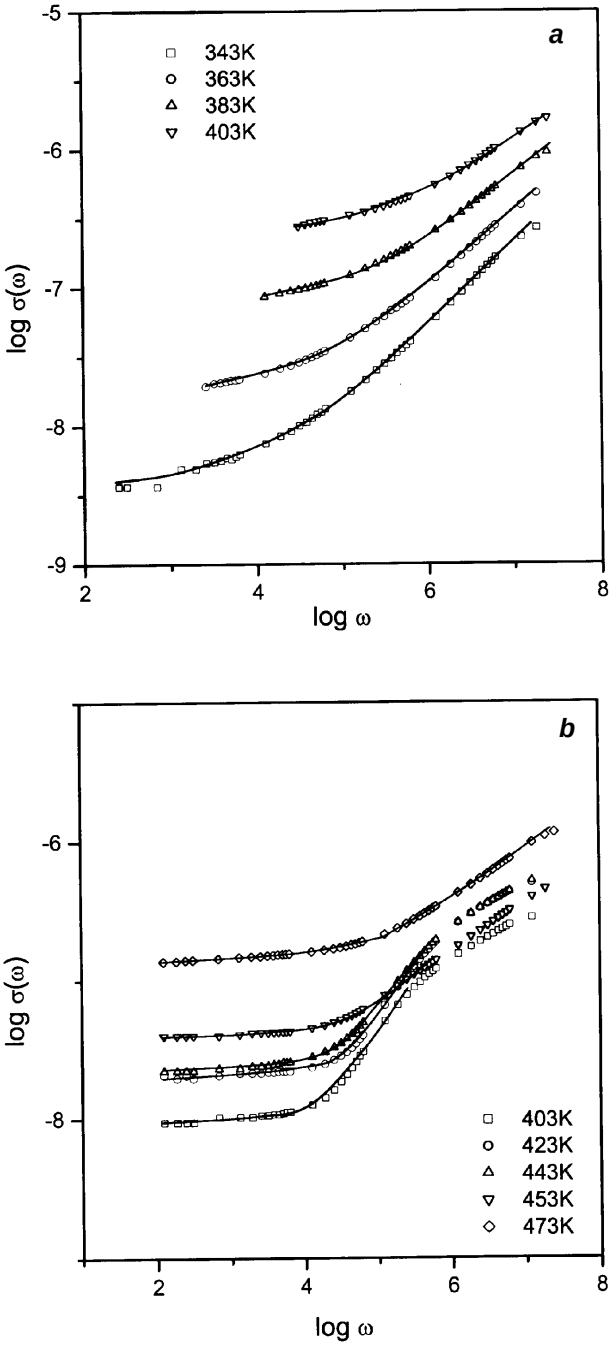

Figure 6. ***a***, Almond–West plot for a typical glass, 00 : 50 : 00, from series A at various temperatures. ***b***, Almond–West plot for a trialkali glass, 10 : 20 : 20, from series B at various temperatures. Solid line is the Almond–West power-law fit.

and *b*) exhibits two regimes of MAE; one between $Na_2(PO_3)_2$ and $(Na\text{-}K)(PO_3)_2$, and the other between $(Na\text{-}K)(PO_3)_2$ and $K_2(PO_3)_2$. It would also appear that such a recognition of two composition regimes would account for the observed MAE. But a closer examination of Figure 4 *a* and *c* makes the above analysis quite inconsistent. The behaviour of log s_{dc} in Figure 4 *c* has a similar shape, but has been tilted in such a way that conductivity at the potassium end is much higher than that at the sodium end. Even if one were to assume that there are two composition regimes and that 20 mol% (of the total alkali) Li_2O present in the system is distributed into two hypothetical subsystems, the fact that the sodium end has a depressed conductivity while the potassium end has an elevated conductivity, is difficult to understand. We may also recognize that, in principle, there are three different alkali couples present in Figure 4 *c*; $(Li_2O/\ Na_2O)\ (PO_3)_2$, $(Li_2O/K_2O)(PO_3)_2$ and $(Na_2O/K_2O)\ (PO_3)_2$, but there is no signature which could even be empirically associated with the presence of three alkali pairs in any of the measured properties. However, the observed behaviour in Figure 4 *a* and *c* itself cannot be understood on the basis of existing theories, because they assume the presence of a common operative conduction barrier and a unique minimum conductivity, although there are two cations having their own dynamics and site descriptions. Among the glasses investigated here, the end members of series B and all the glasses in series A indeed exhibit Arrhenius behaviour (Figure 5 *a*), suggesting that a single, apparent activation barrier is indeed present in all two-alkali compositions. The presence of a single activation barrier is inconsistent if both alkalis were to participate in the transport. This is because if $s = s_A + s_B = s_0^A \exp(-E_A/RT) + s_0^B \exp(-E_B/RT)$, then s cannot be expressed as $s_0 \exp(-E/RT)$. Further, in all two-alkali containing glasses, dielectric relaxation and a.c. conductivity studies also reveal the presence of only a single relaxation peak and a single power law exponent, *s*. Therefore, in simple two-alkali glasses, there must be only one type of charge carrier which determines the magnitudes of charge transport and that cannot be the alkalies.

A new approach to ion transport in oxide glasses

We therefore consider that the primary step in charge transport is associated with the negative charge. The assumption implied in the current theories of ion transport is that alkali ions jump from their positions to equivalent positions, either by thermal fluctuation or under the influence of vanishingly small electrical field. In alkali-containing oxide glasses, this ion jump event is supposed to be followed by a BO–NBO bond switching, which restores status quo ante. It is this approach, which necessitates different barriers for different alkalis. On the other hand, if an alkali ion jump is to be preceded by negative charge transport via a BO–NBO switching (migration of NBO)* and the measured activation barriers can be associated with the BO–NBO switching, restoration of status quo ante in charge distribution in the structure would occur through the follow-up migration of the alkali-ion.

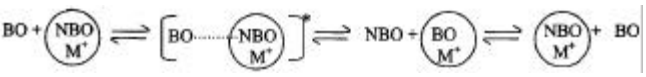

The starred entity corresponds to the activated step and involves rehybridization of phosphorous orbitals in PO_n. Therefore, in a given bialkali glass system there can be only one activation barrier which corresponds to the BO–NBO switching activation and which is characteristic of the composition. Presence of mixed-alkali environment would make BO–NBO switching more difficult because in the activated, rehybridized state the asymmetry of the environment itself can increase the barrier. The two different Voronoi polyhedra[3] associated with the two different alkalis have to undergo shape changes, which manifest as increased barrier.

For the present system of trialkali glasses, it is now easy to understand the presence of two BO–NBO activation barriers because of the presence of two compositional regimes (subsystems) and we need not expect any additional features as a consequence of the presence of three alkali ion pairs. The activation barrier for BO–NBO switching is affected primarily by the magnitude of the redistributable volume around the BO–NBO pair involved in switching. Once the NBO has moved, the coulombic attraction between NBO and the alkali-ion drags the latter to the new position. Since the corresponding barrier is lower than the BO–NBO switching barrier, it does not show up separately. The alkali-ion migration in this approach is thus only a secondary event in ion transport in oxide glasses. Also, any of the alkali ions may migrate to the new position depending upon how low the barrier is at the second stage. We may now see that the higher conductivity and lower activation barrier of the potassium end glass in Figure 4 *c* and *d*, can be attributed to the larger molar volume of this glass which accommodates the activated BO···NBO state with greater ease (see Figure 1 *d*). Suppression of conductivity at the sodium end in spite of the presence of Li_2O is because of the lower molar volume which makes it much more difficult for the primary BO–NBO switching step. The intermediate compositions in series B exhibit two regions in the Arrhenius plot (Figure 5 *b*) consistent with the presence of two subsystems with their own BO–NBO switching dynamics. It may also be noted that higher log s_{dc} at the sodium end in Figure 4 *a* compared to that at the potassium end is also associated

* 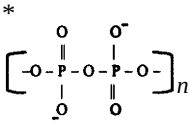

This is a metaphosphate chain; O in =P–O is a bridging oxygen (BO) and O in ≥P–O^- is a non-bridging oxygen (NBO). The reaction is BO (1) + NBO (2) → NBO (1) + BO (2) and occurs between various parts of metaphosphate chains.

with larger structural volume available for BO–NBO switching, as a simple calculation reveals.

The inadequacy of the conventional approach is brought out even more forcefully in dielectric relaxation studies. If dielectric relaxation were to arise from relaxation due to polarization associated with ion jumps, one would expect two relaxation peaks in Li_2O-free glasses (series A). This is clearly absent in the wide range of temperatures and frequencies we have used in these measurements (Figure 7 *c*). Adequacy of a power law with a single exponent, *s*, to account for the a.c. conductivity (Figure 6) and a single stretched exponential function to account for the M″ peaks (Figure 7) is consistent with the presence of a single dominant and leading relaxation event. Indeed, these relaxation peaks have been fitted to stretched exponential functions[19–21] and *b*-values have been determined[22,23] (not reported here). Also, from the temperature dependencies, the activation barrier values, *W*, have been determined (Table 1) which compares well with E_{dc} values. The presence of a single relaxation peak in the present approach can be associated with BO–NBO switching. In trialkali glasses, consistent with the existence of two compositional subsystems, there are two BO–NBO subsystems and therefore they can be expected to give rise to two relaxation peaks and two exponents in Almond–West plots. Indeed, Figures 6 *b*, 7 *c* and *d* clearly demonstrate the existence of two BO–NBO subsystems. The double relaxation peak in Figure 7 *d* observed in trialkali compositions is listed in Table 1. The deconvolution of the relaxation peaks into two subpeaks conforming to two stretched, exponential, relaxation functions[19–21] is beset with inaccuracies, and we have therefore not attempted it. However, the two *s* values have been listed in Table 2 along with other parameters.

Another feature of importance is the temperature behaviour of two relaxation peaks. Physically, each relaxation peak represents the totality of polarization relaxation associated with BO–NBO switching plus that of the associated alkali-ion migration. As the temperature is increased towards the glass transition, it is to be expected that increased-level thermal excitations in two BO–NBO subsystems tend the subsystems to coalesce. When this happens, the differences in the two subsystems disappear and the relaxation peaks merge into a single peak as we approach the glass transition. Indeed, the two peaks merge in the expected manner, as seen in Figure 7 *d*. Correspondingly, at the same temperature, the slopes in the Almond–West plots also merge giving rise to a single *s* value (see Figure 6 *b*). In Figure 8,

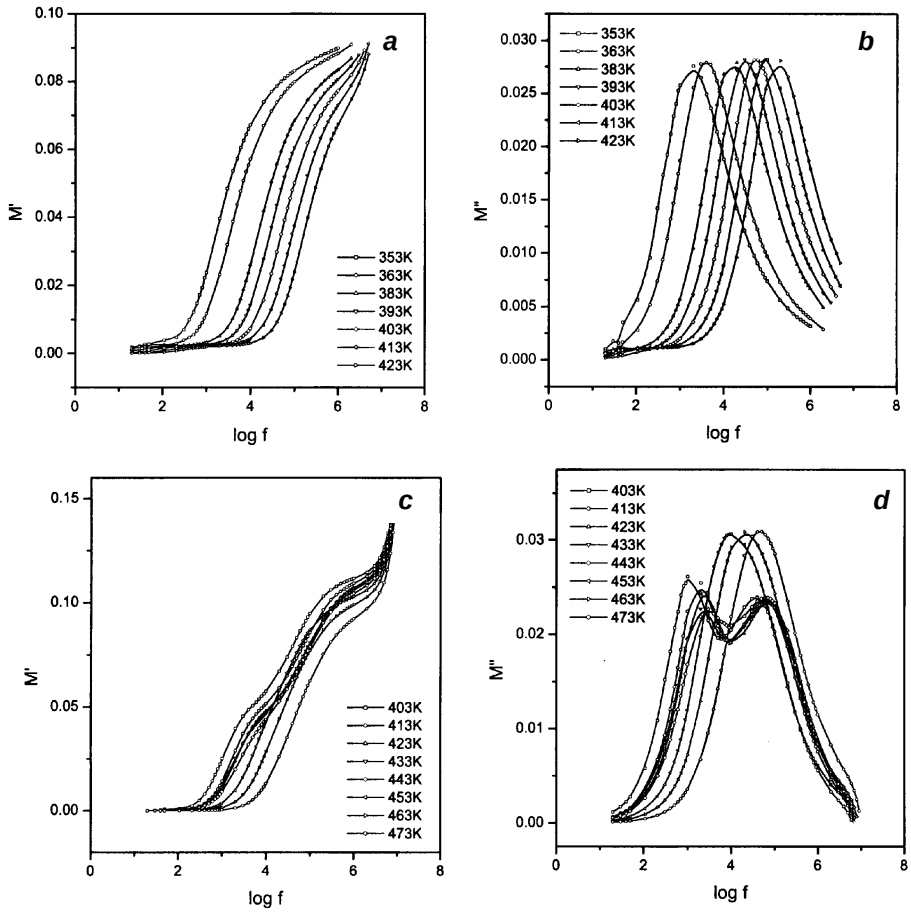

Figure 7. ***a***, Variation of *M′*, and ***b***, *M″* for 00 : 50 : 00 glass from series A as a function of log *f* at various temperatures. Variation of (***c***) *M′* and (***d***) *M″* for 10 : 20 : 20 glass from series B as a function of log *f* at various temperatures.

Table 2. *s* values at different temperatures for 10 : 20 : 20 glass. s_1 and s_2 are the low and high frequency slopes in the *w*-dependent region in Almond–West plots (Figure 6 *b*)

Temperature (K)	s_1 (first)	s_2 (second)	*s* (merged)
403	1.04	0.90	
413	1.06	0.79	
423	0.97	0.67	
433	0.89	0.51	
443	0.84	0.56	
453	0.71	0.60	
463	–	–	0.50
473	–	–	0.51

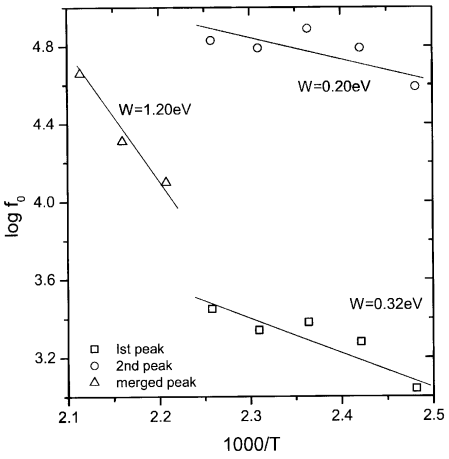

Figure 8. Arrhenius plot of the variation of *M″* peak frequency before and after the merger of two peaks. The activation barrier values (*W*) are indicated on the plot.

we have plotted the logarithmic peak frequency as a function of 1000/*T* and calculated the activation barriers. These activation barriers, *W* (diffusion-less)[24] are also indicated in Figure 8. The observed barriers after the merger of the peak are indeed quite close in magnitude to those determined from the d.c. conductivity listed in Table 1.

Conclusion

The ion-transport behaviour of trialkali metaphosphate glasses has been investigated. Using various experimental techniques, it has been shown that the conventional approach to ion transport is inadequate to understand the experimental observations. It is postulated that charge transport in these glasses occurs through BO–NBO switching as the primary step, which is then followed by alkali-ion migration. Trialkali glasses are unique in that they behave as composites of two subsystems, although there is no evidence of any phase separation. As a consequence, they provide a unique system in which two BO–NBO subsystems are formed, and they exhibit conductivity and relaxation characteristics which are consistent with the proposed transport mechanism. Dielectric relaxation in trialkali glasses is observed as two peaks which merge at higher temperatures close to glass transition.

1. Isard, J. O., The mixed alkali effect in glass. *J. Non-Cryst. Solids*, 1969, **1**, 235.
2. Day, D. E., Mixed alkali glasses: Their properties and uses. *J. Non-Cryst. Solids*, 1976, **21**, 343.
3. Rao, K. J., *Structural Chemistry of Glasses*, Elsevier, Amsterdam, 2002.
4. Stevels, J. M., *Verres Refract.*, 1951, **5**, 4.
5. Mazurin, O. V., *Structure of Glass*, Consultants Bureau, New York, 1965, vol. 4, p. 5.
6. Hendrickson, J. R. and Bray, P. J., A theory for the mixed alkali effect in glasses, Part I. *Phys. Chem. Glasses*, 1972, **13**, 43.
7. Kone, A., Reggiani, J. C. and Souquest, J. L., Thermodynamic approach of the mixed alkali effect in inorganic glasses. *Solid State Ionics*, 1983, **9&10**, 709.
8. Zhong, J. and Bray, P. J., Change in boron coordination in alkali borate glasses and mixed alkali effect, as elucidated by NMR. *J. Non-Cryst. Solids*, 1989, **111**, 67.
9. Maas, P., Bunde, A. and Ingram, M. D., Ion transport anomalies in glasses. *Phys. Rev. Lett.*, 1992, **68**, 3064.
10. Balasubramanian, S. and Rao, K. J., Preferential paths in alkali ion migration and the mixed alkali effect in silicate glasses. *J. Phys. Chem.*, 1993, **97**, 8835.
11. Swenson, J. and Adams, St., Mixed alkali effect in glasses. *Phys. Rev. Lett.*, 2003, **90**, 155507.
12. Greaves, G. N., Gurman, S. J., Catlow, C. R. A., Chadwick, A. V., Houde-Walter, S., Henderson, C. M. B. and Dobson, D. B., A structural basis for ionic diffusion in oxide glasses. *Philos. Mag. A*, 1991, **69**, 1059.
13. Bhat, M. H., Ganguli, M. and Rao, K. J., Mixed alkali effect in boro-tellurite glasses: The primacy of NBO in transport properties. *J. Phys. Chem. B*, (submitted).
14. Almond, D. P., Duncan, G. K. and West, A. R., The determination of hopping rates and carrier concentrations in ionic conductors by a new analysis of ac conductivity. *Solid State Ionics*, 1983, **8**, 159.
15. Almond, D. P., Hunter, C. C. and West, A. R., The extraction of ionic conductivities and hopping rates from ac conductivity data. *J. Mater. Sci.*, 1984, **19**, 3236.
16. Almond, D. P., West, A. R. and Grant, R. J., Temperature dependence of the A.C. conductivity of Na *b*-alumina. *Solid State Commun.*, 1982, **44**, 1277.
17. Sobha, K. C. and Rao, K. J., Investigation of phosphate glasses with general formula $A_xB_yP_3O_{12}$ where A = Li, Na or K and B = Fe, Ga, Ti, Ge, V or Nb. *J. Non-Cryst. Solids*, 1996, **201**, 52.
18. Ito, K., Moynihan, C. T. and Angell, C. A., Thermodynamic determination of fragility in liquids and a fragile-to-strong liquid transition in water. *Nature*, 1999, **398**, 492.
19. Kohlrausch, R., *Pogg. Ann. Phys.*, 1847, **12**, 393.
20. Williams, G. and Watts, D. C., Non-symmetrical dielectric relaxation behaviour arising from a simple empirical decay function. *Trans. Faraday Soc.*, 1970, **66**, 80.
21. Williams, G., Watts, D. C., Dev, S. B. and North, A. M., Further considerations of non-symmetrical dielectric relaxation behaviour arising from a simple empirical decay function. *Trans. Faraday Soc.*, 1971, **67**, 1323.
22. Macedo, P. B., Moynihan, C. T. and Bose, R., The role of ionic diffusion in polarization in vitreous ionic conductors. *Phys. Chem. Glasses*, 1972, **13**, 171.
23. Moynihan, C. T., Boesch, L. P. and Laberge, N. L., Decay function for the electric field relaxation in vitreous ionic conductors. *Phys. Chem. Glasses*, 1973, **14**, 122.
24. Elliott, S. R., Frequency dependent conductivity in ionic glasses: A possible model. *Solid State Ionics*, 1988, **27**, 131.

Received 8 September 2003